Surface & Coatings Technology 401 (2020) 126280

Contents lists available at ScienceDirect

Surface & Coatings Technology

journal homepage: www.elsevier.com/locate/surfcoat

Synthesis and corrosion behavior of cold sprayed dual nanoparticle reinforced Al coatings

Travis Norrell[a], Gehn Ferguson[b], Troy Ansell[a], Tara Saladin[a], Aaron Nardi[b], Andy Nieto[a,*]

[a] Coatings and Composites for Extreme Environments Lab (CE)[2], Department of Mechanical and Aerospace Engineering, Naval Postgraduate School, Monterey, CA 93943, USA

[b] Weapons and Materials Research Directorate (WMRD), US Army Research Laboratory, Aberdeen Proving Ground, MD 21005, USA

ARTICLE INFO

Keywords:
Cold spray
Boron nitride nanoplatelets
Salt fog
Pitting corrosion
Galvanic corrosion

ABSTRACT

This study investigates the synergistic and individual effects of nano boron carbide (nB_4C) and boron nitride nanoplatelets (BNNP) on the corrosion behavior of cold spray aluminum matrix composite (MMC) coatings. Cryomilling and cold spraying were used to synthesize four novel Al MMC coatings with reinforcements consisting of either 2 vol.% nB_4C, 2 vol.% BNNP, or dual nanoparticle reinforcement consisting of 1 vol.% nB_4C plus 1 vol.% BNNP. Cold sprayed coatings were evaluated using microhardness testing which revealed an 11.7% increase in hardness in the dual nanoparticle reinforced composite coating. Coatings were subjected to 500 h and 2000 h corrosion tests in a salt fog chamber consisting of 3.5% NaCl to simulate an aggressive marine environment. Coatings were evaluated post-salt fog chamber by mass and thickness change measurements, optical microscopy, scanning electron microscopy, and energy dispersive spectroscopy. Following 500 h corrosion testing, each composite coating experienced mild to severe pitting throughout a significant portion of the coating. Following 2000 h exposure, in addition to severe pitting, all coatings experienced galvanic corrosion at the coating/substrate interface.

1. Introduction

Cold spray is an additive solid-state powder consolidation process that uses high kinetic energy impact to create coatings, bulk deposits, and near net shape components. [1]. Cold sprayed coatings are inherently appealing for corrosion resistance, because they place a barrier between a substrate requiring protection and a potentially highly oxidizing or corrosive environment. Ngai et al. [2] analyzed the effects of saltwater corrosion on various cold sprayed samples. AA7075 powder was cold sprayed onto an AA7075 substrate and compared to a control substrate during an immersion test, producing significant average pit/pore ratio reduction using He as the carrier gas [2]. In cases where the base material is highly susceptible to corrosion, cold spraying a less corrosive material can produce dramatic results. Cold spraying with relatively noble metals has demonstrated enhanced corrosion properties, showing the versatility of the cold process for depositing well adhered dissimilar materials onto a substrate requiring protection [3]. Diab et al. [4], applied a cold sprayed coating consisting of pure Al onto AZ31B Mg alloy and performed a salt fog chamber accelerated corrosion test over 33 days in accordance with ASTM B117. The bare Mg alloy saw an average weight loss of 90%, compared to < 10% average weight loss for the Al cold sprayed sample [4].

Cold spray can also be used to develop composite coatings with enhanced wear and corrosion resistance, where the selection of reinforcement can be tailored to the application. Ceramic reinforcements are known to enhance the mechanical and wear properties of metal matrix composites. Nieto et al. [5] used various sized B_4C particle reinforced Al composites and found that nanoparticle reinforcements enhanced hardness more than their larger microparticle counterparts. The Al-nB_4C composite had a 56% higher hardness than unreinforced aluminum and 18% higher than Al-μB_4C. Boron nitride nanoplatelets (BNNPs) are another promising ceramic reinforcement, having a two-dimensional structure analogous to graphene. They are exceptionally strong, having an elastic modulus of 700–900 GPa [6]. Additionally, BNNP is chemically inert up to 950 °C, compared to graphene oxidizing around 500 °C [6]. Using these particles as a solid lubricant within a matrix has the potential to increase the tribological properties of a composite material [7–9]. Ceramic 2D nanomaterials such as BNNP offer the possibility of acting as an oxygen barrier in some cases, showing the general promise of 2D nanomaterials [10]. Cold spray is a relatively low-temperature process making it an ideal technique for processing nanocomposite coatings.

* Corresponding author.
E-mail address: Andy.nieto@nps.edu (A. Nieto).

https://doi.org/10.1016/j.surfcoat.2020.126280
Received 7 June 2020; Received in revised form 7 August 2020; Accepted 8 August 2020
Available online 11 August 2020
0257-8972/ Published by Elsevier B.V.

Only a few studies have investigated the use of dual-nanoparticle reinforcements in metallic composites, and none in coating systems [11–16]. Some studies in dual-nanoparticle reinforcements have compared results of two coatings with a set amount of single nanoparticle reinforcement to other coatings with two nanoparticle reinforcements, using a total amount in the dual-system that was higher than that in the single systems [11–14]. Such approaches make it difficult to discern if the use of dual-reinforcements was beneficial or if enhanced properties are due to the higher amount of total reinforcement. Other studies have found using even a small amount of a second reinforcement can greatly increase the mechanical properties of a matrix, such as Mg reinforced with GNPs and CNTs [15,16]. Without increasing the total amount of reinforcements, Polat et al. used B_4C and GNP to reinforce an Al−Si matrix and found synergy between the dual nanoparticles, attributing the majority of the synergy to a more efficient load transfer mechanism [16].

It is proposed here to use a dual-reinforcement approach to develop a composite material that harnesses nano ceramic reinforcements to provide both enhanced hardness and corrosion resistance. Ceramic nanoparticles, such as nB_4C, have been shown to considerably enhanced hardness and wear resistance [5,17]. Likewise, ceramic particles are inert and relatively non-conductive compare with the metal matrix and no galvanic coupling is expected. Instead, as observed previously in Ti-Ta_2O_5 composites the use of inert ceramic particles has been shown to enhance corrosion resistance of the composite [18]. 2D nanoceramics have the additional potential mechanism of wrapping around grains and hindering diffusion thru grain boundaries [19], which can both enhance hardness by suppressing grain growth and prevent diffusion of oxidizing species. The present research utilized 2 vol.% total reinforcements in all coatings as literature on nanocomposite indicates this is a sufficient loading to induce strengthening, while avoid agglomeration issues. The effect of dual reinforcements on hardness and corrosion resistance in a simulated austere marine environment was compared to the properties wrought by a single reinforcement.

2. Methods and materials

2.1. Materials

Base powder for the composites consisted of cold spray grade commercially pure Al from Centerline Limited (SST5001, Windsor, ON, Canada). The powders were spherical and had an average particle diameter of 27.4 μm (Fig. 1a). Nano boron carbide (nB_4C) of > 99% purity from US Research Nanomaterials, Inc. (US2140, Houston, TX, USA) was used. The nB_4C particles ranged from 10 to 50 nm in diameter (Fig. 1b). Boron nitride nanoplatelets (BNNP) of 99.5% purity from SkySpring Nanomaterials (1523DX, Houston, TX, USA) were utilized. BNNP had an average length of 2.1 μm and were only a few tens of nm thick. Fig. 1c is an SEM image of BNNP showing multiple layers stacked and folded together. BNNPs fold over at high angles without fracturing, indicating their intrinsic flexibility and toughness Fig. 1d is a TEM image of BNNPs, with the red circle highlighting folds in the BNNP. Tough ceramic nanoparticles are ideal materials for enhancing strength and toughness in composites. Composition A is the control, consisting of only Al. Composition A-C contains only boron carbide reinforcement, specifically 98% Al + 2% nB_4C. Composition A-N contains only boron nitride reinforcement, specifically 98% Al + 2% BNNP. Compositions containing both carbide and nitride reinforcements, specifically 98% Al + 1%nB_4C + 1% BNNP, are denoted as A-CN. Powder processing for A-CN was done in a single mixing step. A-CN-m is the same composition as A-CN, but mixing was conducted in multiple steps, described in the next subsection. All composites had a total reinforcement of 2 vol.%. Compositions of the powders synthesized and subsequent coatings fabricated and investigated are provided in Table 1.

2.2. Composite processing

To synthesize the composite powders for cold spray, Al and nanomaterial reinforcements were mixed via cryomilling (Spex 6870 Freezer/Mill, Metuchen, NJ, USA). All five powders (including pure Al) were cryomilled for five cycles, where each cycle consisted of two minutes on followed by two minutes off. The two minutes spent off were an additional measure taken to ensure the temperature inside the sealed tube did not rise considerably and result in growth or agglomeration of nanoparticles, or distortion of the spherical Al powder. Powders A, A-C, A-N, and A-CN were mixed and Cryomilled together. Powder A-CN-m has identical composition to A-CN but processing consisted of two milling steps. This composite mixed Al + 2vol.%nB_4C and Al + 2vol.%BNNP in separate cryomilling runs, same cycles as before. The individually Cryomilled powders were then mixed together using a high energy ball mill (HEBM, SPEX 8000) for five minutes without any milling media. All composite powders were passed through a 100 μm sieve to filter out any larger particles that may have formed during the mixing process that could adversely affect the flowability of the powder during cold spraying.

AA6061 substrates (13 mm × 25 mm × 152 mm) were cleaned and grit blasted using ~40 μm Al_2O_3 particulates. The cryomilled cold spray feedstock powders were sprayed onto the prepared AA6061 substrates using a VRC Gen 3 system (VRC Metal Systems, Rapid City, SD, USA) with a target thickness of 250 μm. Prior to cold spray deposition, the powders were dried out in a pre-heating oven to drive off moisture and were shaken to break up any agglomerated particles. This was done to improve how well the powders feed in the powder feeder. The He carrier gas was driven at 3.45 MPa, and the gas temperature was 425 °C. The gun rastered at 200 mm/s over the substrate with a line spacing of 0.5 mm. The coatings were applied in 2 passes. These parameters were developed at US ARL and were targeted for attaining good spray quality of aluminum coatings. Additional substrate specimens with the same dimensions and surface preparation were also sprayed with the gun constantly traveling over the substrate for 30 passes to measure deposit efficiency (DE). A scale with ± 0.1 g precision was used for DE measurements. The mass of powder and the mass of the substrate were measured before and after the spray and were used to determine powder deposit efficiency.

2.3. Salt fog chamber testing

Accelerated corrosion tests on the coatings were conducted using a salt fog chamber with a 3.5 wt.% NaCl solution, which is the average salinity of seawater. Otherwise, salt fog chamber testing was conducted largely in accordance with ASTM B117 [20]. The samples were held in place by a custom 3D printed polylactic acid (PLA) tray. The PLA tray held the samples at 20 degrees from the vertical and contained a drainage cavity below to prevent water buildup that would lead to immersion conditions. One set of specimens was exposed for 500 h and another was exposed for 2000 h, in order to track the evolution of corrosion attack mechanisms over time. Mass and thickness change measurements were conducted on a weekly basis.

2.4. Characterization

As-sprayed samples and both sets of corrosion samples were sectioned, cold mounted, and ground using 120-, 400-, 800-, 1200-grit SiC paper and then polished using a 1 μm Al_2O_3 solution. Etching of the samples was performed using Kellers reagent (1% HF, 1.5% HCl, 2.5% HNO_3, balance water). Brightfield and darkfield optical microscopy (OM) was performed using a Nikon Epiphot 200 optical microscope. Scanning electron microscopy (SEM) was performed using a Zeiss Neon 40 dual beam FIB-SEM (White Plains, NY, USA). SEM imaging was performed using an accelerating voltage ranging from 2 kV to 20 kV at a working distance of 5 mm. In order to prevent charging of corrosion

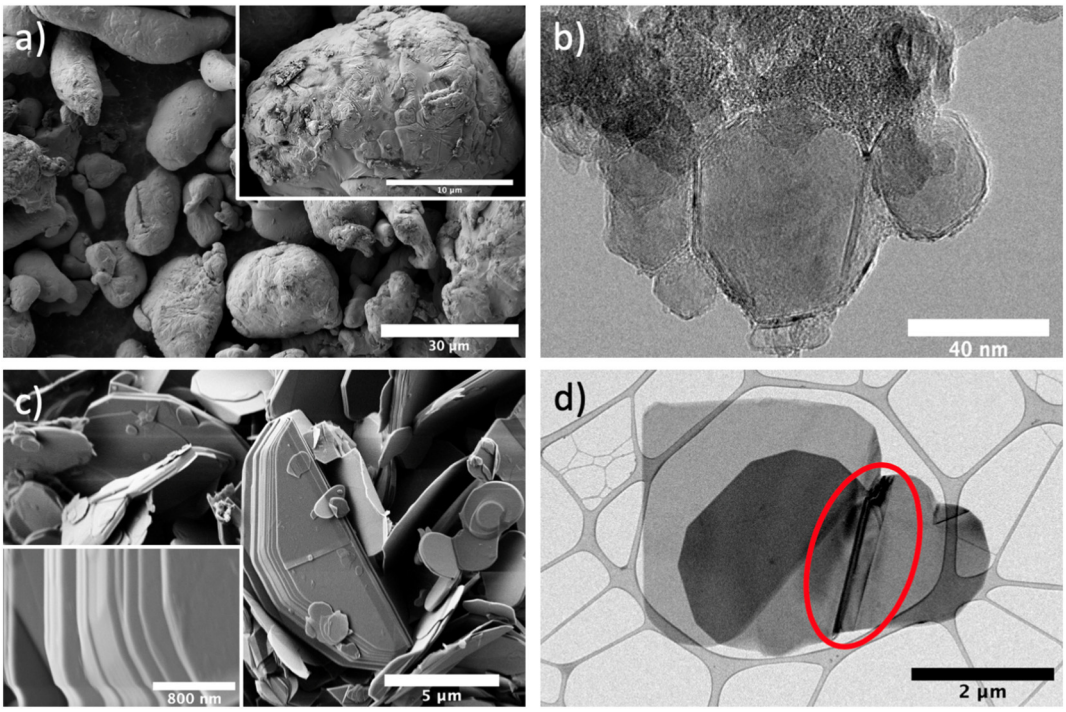

Fig. 1. a) SEM image of commercially pure aluminum cold spray powder (inset: surface of single Al particulate), b) TEM image of nB_4C, c) SEM image of multiple BNNPs, many folded over each other (inset: individual BN layers in BNNP), and d) TEM image of BNNP. Red circle in d) shows BNNP folded over itself indicating flexibility and intrinsic toughness of the 2D nanomaterial. (For interpretation of the references to color in this figure legend, the reader is referred to the web version of this article.)

Table 1
Summary of coatings.

Composition (vol.%)	Nomenclature	Powder processing method
100% Al	A	Cryomilling
98% Al + 2% nB_4C	A-C	Cryomilling
98% Al + 2% BNNP	A-N	Cryomilling
98% Al + 1% nB_4C + 1% BNNP	A-CN	Single cryomilling (Al + nB_4C + BNNP)
98% Al + 1% nB_4C + 1% BNNP	A-CN-m	Individual cryomilling + final HEBM mixing

products, specimens were sputter coated with a thin Pt/Pd layer using a Cressington 208HR sputter coater (Liverpool, UK). Two cross sections were looked at for the 2000 h samples to ensure generalization of observations and trends. A Struers DuraScan hardness tester (Cleveland, OH) was used to conduct microhardness tests using a load of 0.9807 N. Ten individual hardness measurements were taken on each sample to attain a statistically significant sample. A Rigaku MiniFlex 600 X-ray diffractometer (XRD) (Tokyo, Japan) with an excitation voltage of 40 kV and a current of 15 mA was used to confirm chemical identity of corrosion products.

3. Results and discussion

3.1. Nanocomposite powder synthesis

The nB_4C appear to be adequately dispersed in the A-C composite powder by the cryomilling process as the nanoparticles can be seen to uniformly coat the surface of the large Al particulates (Fig. 2a.) The nB_4C is intimately adhered to the large aluminum particles via Van der Waals forces induced by the high specific surface area of the nanoparticles. BNNPs in the A-N composite powder are indicated by red circles in Fig. 2b. It is clear that cryomilling preserves the overall platelet structure of the BNNP and also thoroughly mixes the BNNP with Al. Mechanical adhesion (from localized impact during milling) and Van der Waals forces are the dominant forces maintaining the contact between BNNP and Al. Because of their larger size and aspect ratio, the BNNP do not coat the surface of the Al particles in the same manner as the nB_4C. A few BNNPs are observed to remain unattached to any Al particulates.

3.2. Coating deposition efficiency, microstructure & microhardness

The coating deposit efficiencies are presented in Table 2 and were calculated using Eq. (1). The average thickness and hardness values of each coating are presented in Table 3, with the error range representing one standard deviation. Coating A-N, which contains the highest amount of BNNP, was a substantially thinner coating compared to the other four samples. Given that spraying parameters were unchanged across compositions, and the higher measured deposition efficiency (DE) of the powder, this was an unexpected result. A source of error in DE measurements is powder being left in the powder hopper and in the feed lines. Coating A-CN-m is the thickest, indicating that use of dual nanoparticles and an additional ball milling step enhanced the deposition efficiency of this powder which is supported by Table 2.

$$Deposition\ Efficiency\% = \frac{Substrate\ Mass_{final} - Substrate\ Mass_{initial}}{Powder\ Mass_{initial} - Powder\ Mass_{final}} * 100 \quad (1)$$

The cause for the relative ineffectiveness of A-N powder in building up a thick coating could be attributed to the relatively higher BNNP content compared to the other composites. BNNP may create a thermal barrier to the Al feedstock reaching the necessary temperature for sufficient softening and subsequent strong bonding between the feedstock and substrate [21]. If the BNNP wrap around an Al particulate, they may act as a thermal barrier between the hot carrier gas and the Al particulates. [22], effectively stopping the hot gas from reaching the Al and heating sufficiently [23]. This adverse effect is absent in the dual-

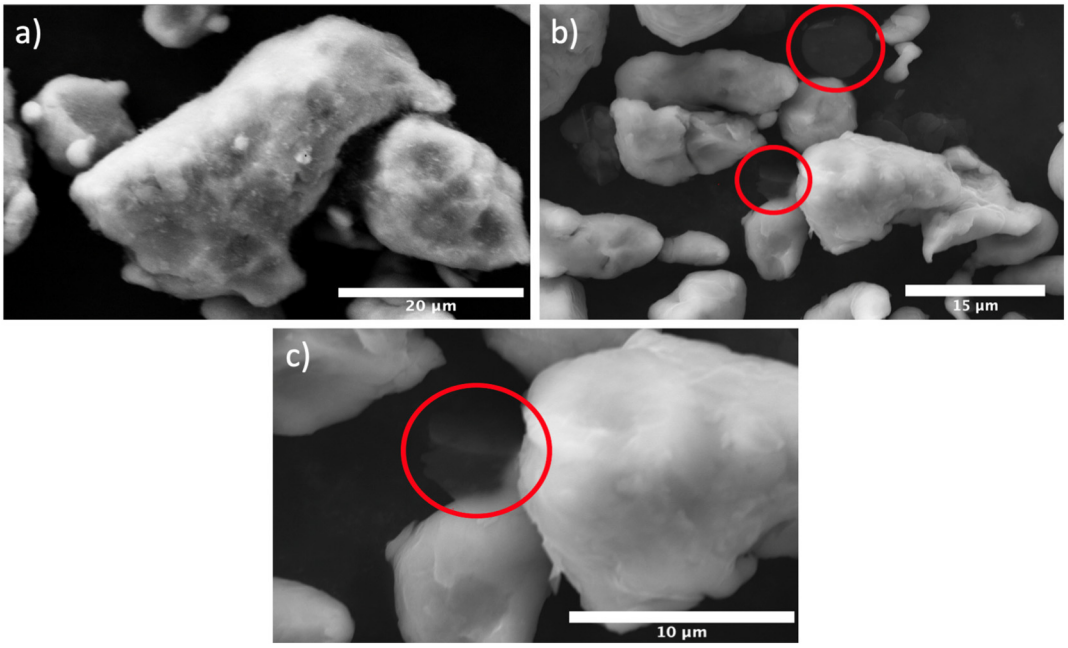

Fig. 2. SEM images of a) nB_4C coating Al within powder A-C, b, c) BNNP adhered to Al within powder A-N.

Table 2
Deposition efficiency for each coating.

Coating	Deposition efficiency
A	73.8%
A-C	64.5%
A-N	79.6%
A-CN	69.4%
A-CN-m	79.6%

Table 3
Average thickness and microhardness for each coating.

Coating	Thickness (μm)	Hardness (HV)
A	271 ± 25	57 ± 2
A-C	324 ± 16	57 ± 4
A-N	164 ± 10	61 ± 3
A-CN	322 ± 17	64 ± 3
A-CN-m	412 ± 39	63 ± 5

reinforcement coatings that contain relatively less BNNP, indicating there may be a threshold content of BNNP that adversely affects heat transfer. The dual-reinforcement composites contain only 0.5 vol.% BNNP, indicating the threshold to be 0.5–1.0 vol.%. The same effect is not expected for nB_4C, as their low aspect ratio does not enable a continuous thermal barrier. Further studies are planned to elucidate coating deposition and build-up efficiency.

Powders deposited during cold spray undergo severe plastic deformation, creating layers of splats that make up the deposit or coating on the substrate. The splats boundaries are visible for coatings A and A-N in Fig. 3a and b, respectively. Adding BNNP or nB_4C does not appear to significantly distort the shape or alter size of splats within the microstructure. Dual-reinforcements also did not noticeably impact the microstructure. Fig. 3c–d are SEM images of BNNP within the cold sprayed coating, protruding from the sample cross section. SEM confirms retention of BNNP after cold spraying and it appears that the BNNP retains its overall size and shape. Fig. 3e–f shows another instance of BNNP bridging two splat boundaries. Minimal damage and retention of the high aspect ratio make it more likely that BNNPs would assist in pinning dislocations, increasing hardness, and serving as a protective barrier within the composite. The nanometric size of nB_4C made it difficult to observe within coating microstructure.

It does not appear that adding nB_4C alone provides any benefit with regards to increasing hardness, but adding BNNP alone does improve the hardness noticeably. Of important note, both coatings that contain dual reinforcement nanoparticles demonstrated improved hardness over the control and single reinforcement coatings, indicating a synergistic effect between the nB_4C and BNNP when added to the same coatings. Specifically, coating A-CN achieves a nearly 12% increase in hardness. This can be explained in terms of the shear lag theory for load transfer in composites [16]. The nB_4C adhering to the Al and BNNP serve to enhance mechanical interlocking, thereby enhancing load transfer mechanisms to the strong and high aspect ratio 2D BNNP reinforcement and increasing frictional resistance to BNNP pull-out. High aspect ratio particles are known to be more effective at transferring loads under shear lag theory. In contrast, strengthening from 0D nanoparticles such as nB_4C is typically achieved from Orowan strengthening that requires coherent interfaces within the grains to inhibit dislocation movement. In the present coatings nB_4C are mostly present at splat boundaries, where porosity exists and dislocations would be pinned anyway, and hence nB_4C appear to be ineffective at strengthening.

3.3. 500 h Salt fog exposure

Every sample exhibits an increase in mass and thickness (Table 4), indicating an oxide layer forming on the surface of each coating. Oxide layers create an area of passivity and greatly reduce the amount of corrosion that occurs on a surface, and the mass gain and thickness gain is indicative of how much of a passive oxide layer is formed. While an oxide layer is protective in nature, it still represents a loss of material *(metal coating)* on the surface and corrosion of the metal. Coating A-C exhibits the highest mass gain and thickness gain for both 500 h and 2000 h exposures, indicating the relatively poor uniform corrosion resistance. The mechanism is still unclear, but the nanometric size of nB_4C may increase its activity and make it more prone corrosion reactions, despite the inert characteristics of bulk B_4C. Composites with BNNP show comparable changes in mass and thickness to pure Al sample, indicating that BNNP-containing nanocomposites retain the

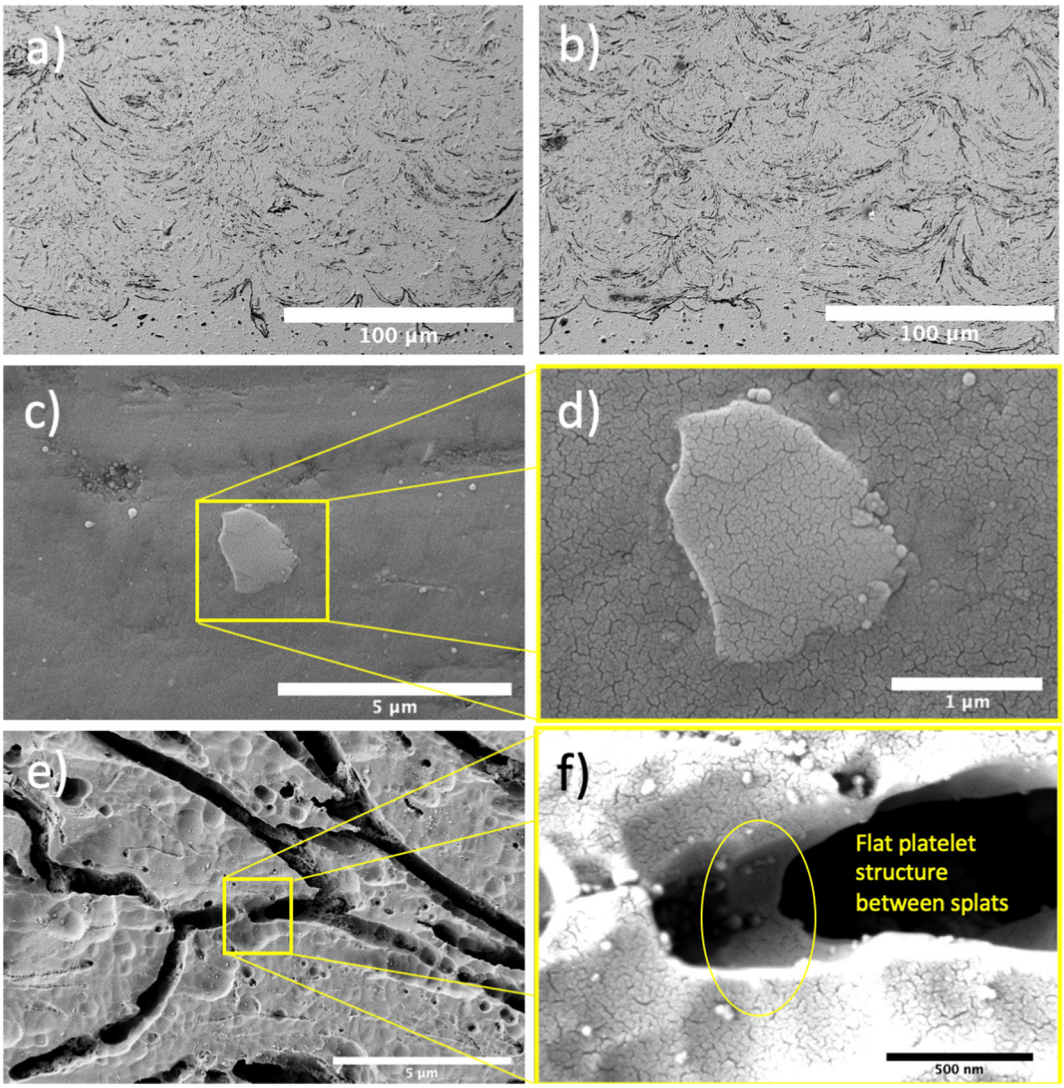

Fig. 3. SEM images of a) coating A and b) coating A-N showing similar shaped splat boundaries, c) SEM images of BNNP within cold sprayed coating at intermediate magnification and d) high magnification, e, f) SEM images of BNNP visible between splat boundaries. Cracks and lighter colored circles visible in c) and d) are artifacts of sputtering.

Table 4
Mass and thickness changes of coatings after 500-h and 2000-h salt fog exposures.

Sample	Δm_{500} (g)	Δm_{2000} (g)	Δt_{500} (mm)	Δt_{2000} (mm)
A	+0.10	+0.09	+0.10	+0.31
A-C	+0.35	+0.50	+0.40	+0.86
A-N	+0.12	+0.13	+0.10	+0.17
A-CN	+0.12	+0.18	+0.20	+0.41
A-CN-m	+0.09	+0.16	+0.10	+0.30

excellent corrosion resistance of Al. The dual reinforced coating (A-CN-m) that underwent cryomilling and HEBM processing may have better overall dispersion that leads to less areas where only nB_4C is present. In contrast, localized areas rich in nB_4C may explain why A-CN (processed only by cryomilling) exhibited the highest mass and thickness changes of any of the BNNP containing composites.

Aside from uniform corrosion, it is critically important in coatings to characterize localized corrosion, which could lead to substrate attack prior to noticeable mass or thickness changes. In Fig. 4a, coating A shows no pitting across the entire cross section in that representative light micrograph of the cross section. In Fig. 4b, pitting corrosion has traversed over halfway through coating A-N after only 500 h of salt fog chamber testing. It appears that corrosion starts on the left side of Fig. 4b then undercuts through the uppermost part of the coating and leads to souring conditions within the pit. To understand what is occurring at the surface of the coating, it is important to consider the overall corrosion as having two different mechanisms – the initiation of corrosion and the propagation of corrosion through the coating via pitting. Pitting occurs by the following reactions of aluminum in a chloride environment at the anodic site [24]:

$$Al(s) \leftrightarrow Al^{3+}(aq) + 3e^{-} \quad (2)$$

$$Al^{3+}(aq) + 4Cl^{-}(aq) \leftrightarrow AlCl_4^{-}(aq) \quad (3)$$

And at the cathodic site [24]:

$$\frac{1}{2}O_2 + H_2O + e^{-} \leftrightarrow OH_{ads} + OH^{-} \quad (4)$$

The presence of pitting in the composite coatings is attributed to a micro-crevice corrosion, stemming from increased surface roughness, which is known to severely increase pitting corrosion [25]. Nanocomposites often exhibit greater surface roughness due to protruding particulates. One study looked at the effect of adding GNP to Al_2O_3 and found that a higher concentration of nanoparticles increased the surface

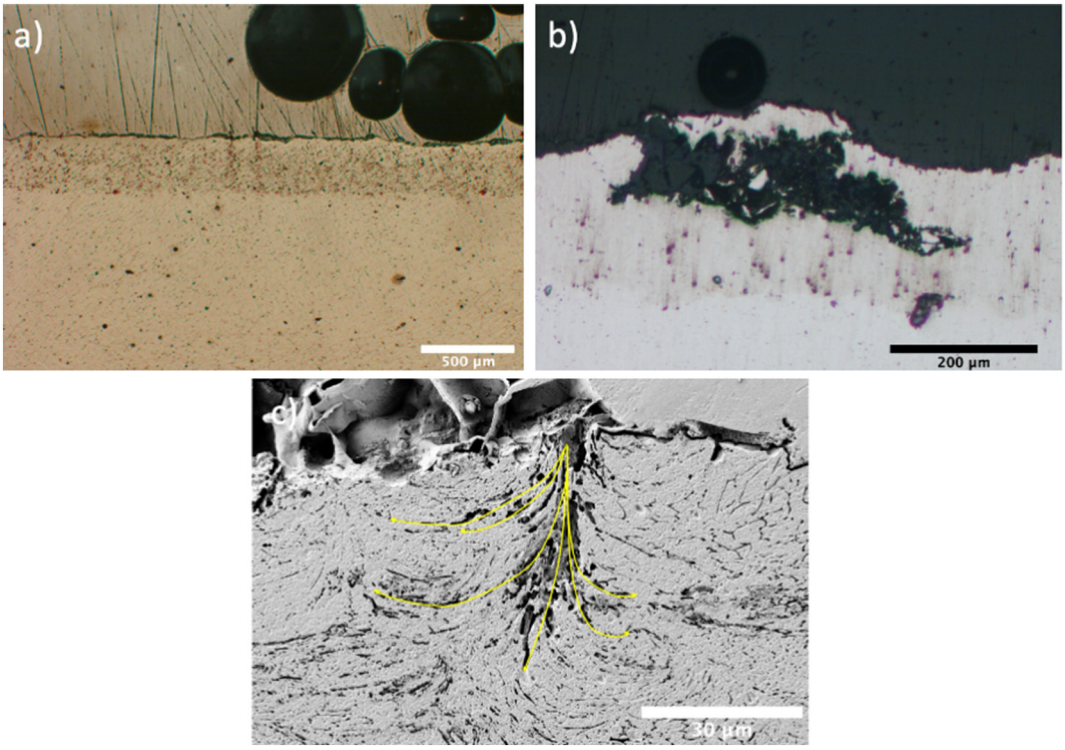

Fig. 4. a) OM bright-field (BF) micrograph of coating A demonstrating strong corrosion resistance, b) OM BF micrograph of coating A-N showing severe pitting traversing nearly half the coating thickness, and c) SEM of pitting in coating A-C following 500 h exposure.

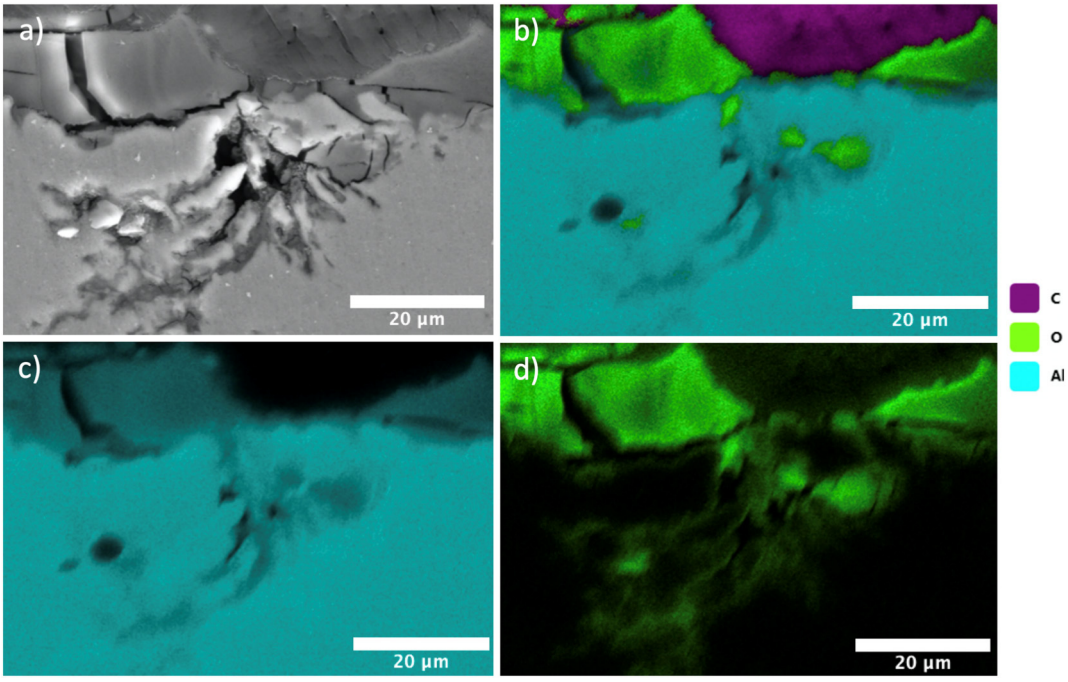

Fig. 5. a) SEM image of pitting within reinforced coating, b) all EDS elemental overlay, c) only Al, and d) only O, showing a lack of Al_2O_3 over the entrance to the pit in the coating. A lack of protective oxide layer facilitates the onset of pitting corrosion within the coating.

roughness of the composite significantly [26]. Another study varied the amount of TiO_2 nanoparticles within a polymer and saw close to a linear increase in the surface roughness compared to the control [27]. The presence of nB_4C and BNNP likely lead to localized increases in surface roughness as well. The high aspect ratio of BNNP may make them especially prone to forming micro-crevices that initiate corrosion.

Metal ions build up under an area of low flow within a micro-crevice, leading to localized souring. Additionally, oxygen is consumed in the cathodic reaction and may not be easily replenished within a micro-crevice or formed pit. This creates an oxygen concentration gradient between the surface and the micro-crevice, resulting in the flow of current, further exacerbating corrosion within the micro-crevice. Furthermore, the small size of the micro-crevice leads to a small anode to cathode ratio, further exacerbating the growth of the pit.

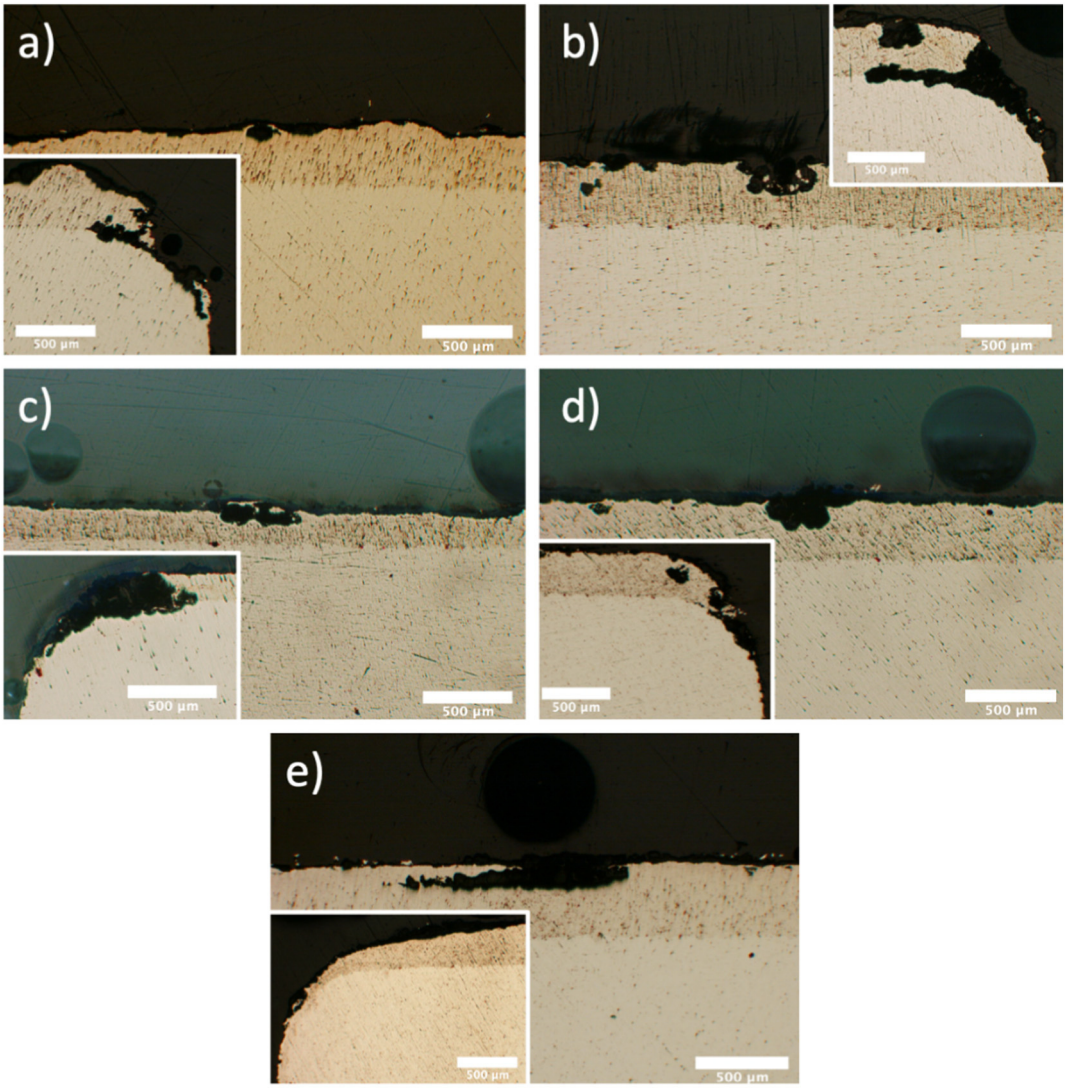

Fig. 6. OM BF micrographs of a) coating A bulk, b) coating A-C bulk, c) coating A-N bulk, d) coating A-CN bulk, and e) coating A-CN-m bulk, showing extensive pitting and galvanic corrosion following 2000 h in a salt fog chamber (insets showing coating edge).

Although all of the coatings containing nanoparticles exhibit increased pitting corrosion, coating A-N which contained the largest amount of BNNP yielded the deepest pit of all the coatings, demonstrating the potential impact the BNNP induced micro-crevices have on pitting corrosion initiation.

Fig. 5 shows a pit representative of those typically found in the composite coatings. There is an oxide layer in Fig. 5a that is approximately 15–20 µm in thickness. In Fig. 5a, there is a clear entrance to the pit in the coating that corresponds to a lack of oxygen depicted in Fig. 5d. If there were a continuous oxide coating through the entire surface, it is unlikely that severe pitting would have occurred. It appears that the presence of ceramic nanoparticles within the composites interferes with the formation of a cohesive protective oxide layer. If ceramic nanoparticles interrupt the contiguous formation of a protective oxide layer in some cases, as appears to be the case in Fig. 5, a complete absence of the film locally is expected to lead to rapid anodic dissolution of the aluminum metal. In addition to EDS elemental mapping, XRD phase analysis (not shown) confirms that the primary corrosion product is Al_2O_3.

The pitting pattern Fig. 5a also closely matches “corrosion tunneling” observed by Xie et al. [28]. In that study, the authors observed a tortuous path of corrosion tunneling into a cold sprayed zinc coating during an immersion test with 3.5 wt.% NaCl solution. The presence of multiple tortuous paths in the study was a result of extensive plastic deformation resulting from the cold spray process. Tunneling through the coating allowed the electrolyte to penetrate farther into the coating and aided in the pitting corrosion already discussed. Greater porosity would also be more conducive to a facile corrosion path thru splat boundaries, due to electrolyte infiltration.

3.4. 2000 h Salt fog exposure

After 2000 h of salt fog exposure, coating A retained the lowest mass gain out of all the samples. The composite coatings consistently undergo more severe uniform and localized corrosion. Fig. 6 shows light micrographs of the coatings post 2000 h salt fog exposure. While

coating A appears nearly pristine across the entire length of the cross section observed in the 500 h test, a single pit was observed across both 2000 h cross sections. Per the mechanism of corrosion proposed for the 500 h exposures, there should be minimal pitting in the pure Al coating in a longer duration corrosion test because there are no nanoparticles within the coating to disrupt the protective oxide film formation or to induce significant micro-crevice corrosion. However, the inherent roughness produced during the cold spray deposition is sufficient to induce some localized pitting corrosion during longer duration exposures.

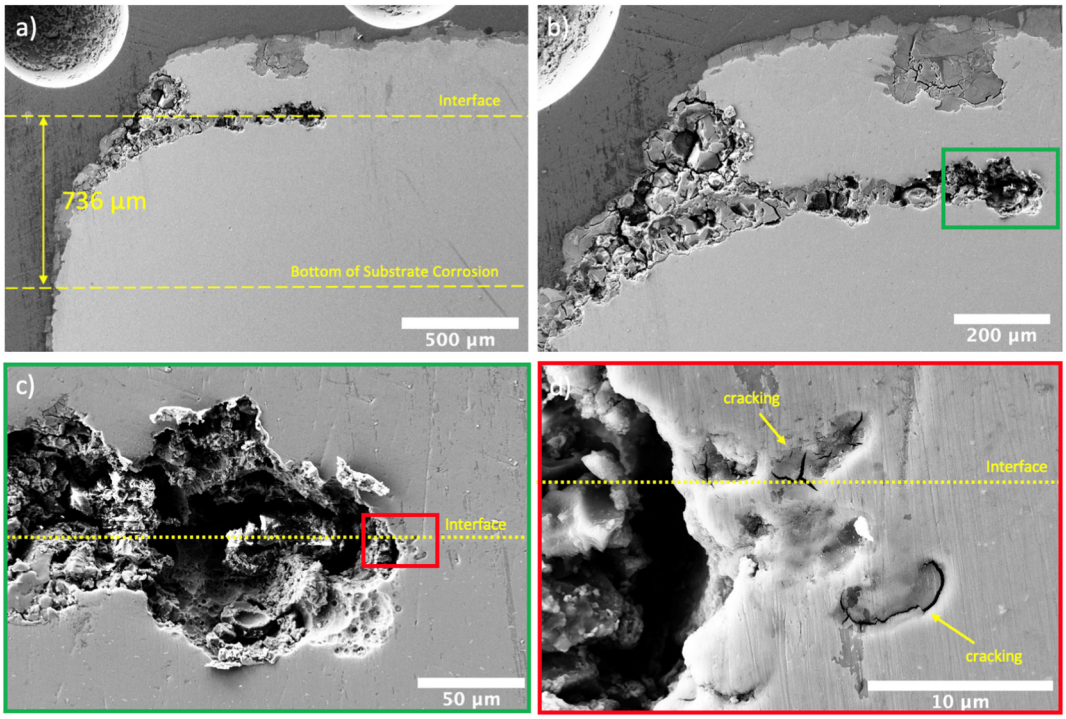

Fig. 7. SEM images of coating A-C following 2000 h in salt fog corrosion chamber showing a) corrosion of the AA6061 substrate, b) galvanic and pitting corrosion along coating/substrate interface at low magnification, c) intermediate magnification, and d) high magnification. In d), cracking at the leading edge of corrosion along the interface is visible. The optical and SEM images are flipped 180 degrees horizontally because of the reflection occurring within the optical microscope.

A primary distinction between the 500 h and 2000 h corrosion tests is extensive corrosion along the coating/substrate interface in most of the specimens exposed for 2000 h. In Fig. 7, there is significant corrosion eating away at both the metal and the substrate. This is initiated by galvanic corrosion at the interface. Galvanic corrosion initiates micro-crevices at the coating/substrate interface that then become active pitting sites. After initiation, corrosion becomes severe due to simultaneous pitting and galvanic corrosion at the interface.

Fig. 7b–d presents the corrosion of coating A-C at interface of the coating and substrate, stemming from the galvanic mismatch between AA6061 alloy and the commercially pure Al matrix of the composite coatings. Throughout the area corroded in Fig. 7a, there is extensive cracking of the formed aluminum oxide. In Fig. 7c, corrosion is oxidizing the metal coating and metal substrate in approximately equal amounts above and below the interface. As the galvanic corrosion progresses through the interface, it is not migrating either above or below the interface line - instead it proceeds along the interface line where there is the electric potential difference between the coating and substrate. Fig. 7d is a high magnification image of the leading tip of the corrosion focusing at the interface, showing where the metal has started to oxidize. This indicates that aluminum oxide is formed immediately around the sites of aluminum corrosion but that it was not necessarily protective because of the presence of chlorides in an aerated environment [29].

Coating A-N in Fig. 6c can be considered a more advanced stage of the corrosion depicted in coating A-C, Fig. 6b. In coating A-N, the pit forms on top of the coating and traverses through the coating down to the area initiated by galvanic corrosion and causes a portion of the coating to detach completely. At this point, the area previously covered by the coating is completely exposed to the corrosive environment.

Not only does galvanic corrosion degrade the coating, but it also initiates corrosion of the substrate as shown in Fig. 7a. Fig. 7a shows corrosion of the AA6061 substrate 736 µm down from the interface of the coating and substrate. Closer to the interface, there is more extensive corrosion of the substrate. Further from the interface, there is minimal corrosion of the substrate, thereby indicating that the corrosion of the substrate is correlated to its proximity to the interface and hence very likely a result of galvanic corrosion.

4. Conclusions

Aluminum coatings reinforced with nB_4C, BNNP, and dual nanoparticle reinforcements are fabricated using cold spray. Equal amounts of total reinforcement are used in all composites in order to determine whether the use of dual nanoparticle reinforcements is advantageous over any single particle. Reinforcing commercially pure aluminum with only 2% ceramic nanoparticles proves to bolster the hardness of the matrix by nearly 12% for the dual reinforced Coating A-CN. BNNP containing coatings retained the excellent uniform corrosion resistance of Al. However, incorporating nanoparticles have a significant drawback, in that every coating with nanoparticle reinforcements demonstrates a higher susceptibility to pitting corrosion when exposed to a simulated marine environment. The presence of nanoparticles interrupts the formation of the protective Al_2O_3 film, leading to localized corrosion, where a small anode to cathode ratio will exacerbate pitting corrosion. Nanoparticles are known to increase surface area, which further increases propensity for micro-crevice and subsequent pitting corrosion. The high aspect ratio of BNNP may make them especially prone to forming localized micro-crevices that can initiate pitting corrosion. Longer duration (2000 h) exposure revealed a corrosion mechanism not previously reported in cold sprayed coatings. Galvanic corrosion was seen to occur, despite both substrate and coating being Al-based. Galvanic corrosion then leads to significant corrosion of the more active substrate metal, the 6061 alloy. Galvanic corrosion is seen in all coatings, however, the presence of BNNP may again produce localized micro-crevices that amplify the degree of pitting.

CRediT authorship contribution statement

Travis Norrell: Data curation, Formal analysis, Investigation,

Methodology, Validation, Visualization, Writing - original draft.**Gehn Ferguson**:Investigation, Methodology, Validation, Writing - original draft.**Troy Ansell**:Formal analysis, Investigation, Validation, Writing - review & editing.**Tara Saladin**:Data curation, Investigation.**Aaron Nardi**:Investigation, Methodology, Resources, Writing - review & editing.**Andy Nieto**:Conceptualization, Investigation, Methodology, Project administration, Resources, Supervision, Writing - review & editing.

Declaration of competing interest

The authors declare that they have no known competing financial interests or personal relationships that could have appeared to influence the work reported in this paper.

Acknowledgments

AN acknowledges support from the Naval Postgraduate School thru the Research Initiation Program (RIP) and from the NPS Foundation thru a SEED Phase II grant.

References

[1] R. Raoelison, Y.S.T. Xie, M. Planche, R. Kromer, S. Costil, C. Langlade, Cold gas dynamic spray technology: a comprehensive review of processing conditions for various technological developments till to date, Additive Manufacturing 19 (2018) 134–159.
[2] S. Ngai, T. Ngai, F. Vogel, W. Story, G.B. Thompson, L.N. Brewer, Saltwater corrosion behavior of cold sprayed AA7075 aluminum alloy coatings, Corros. Sci. 130 (2018) 231–240.
[3] S.M. Hassani-Gangaraj, A. Moridi, M. Guagliano, Critical review of corrosion by cold spray coatings, Surf. Eng. 31 (2015) 803–815.
[4] M. Diab, X. Pang, H. Jahed, The effect of pure aluminum cold spray coating on corrosion and corrosion fatigue of magnesium (3% Al-1% Zn) extrusion, Surface Coatings and Technology 309 (2017) 423–435.
[5] A. Nieto, H. Yang, L. Jiang, J.M. Schoenung, Reinforcement size effects on the abrasive wear of boron carbide reinforced aluminum composites, Wear 390-391 (2017) 228–235.
[6] Y. Song, G. He, Y. Wang, Y. Chen, Tribological behavior of boron nitride nanoplatelet reinforced Ni_3Al intermetallic matrix composite fabricated by selective laser melting, Mater. Des. 165 (2019).
[7] B. Lee, D. Lee, J.H. Lee, H.J. Ryu, S.H. Hong, Enhancement of toughness and wear resistance in boron nitride nanoplatelet (BNNP) reinforced Si_3N_4 nanocomposites, Sci. Rep. 6 (2016).
[8] C. Zhang, A. Nieto, A. Agarwal, Ultrathin graphene tribofilm formation during wear of Al_2O_3-graphene composites, Nanomaterials and Energy 5 (2016) 1–9.
[9] A. Nieto, The promise of 2D nanolaminated materials as protective solid-state lubricants, Lubricants 8 (2020).
[10] A. Nieto, A. Kumar, D. Lahiri, C. Zhang, S. Seal, A. Agarwal, Oxidation behavior of graphene nanoplatelets reinforced tantalum carbide composites in high temperature plasma flow, Carbon 67 (2014) 398–408.
[11] H. Kwon, G. Lee, S. Kim, B. Lee, W. Seo, M. Leparoux, Mechanical properties of nanodiamond and multi-walled carbon nanotubes dual-reinforced aluminum matrix composite materials, Mater. Sci. Eng. 632 (2015) 72–77.
[12] H. Kwon, S. Cho, M. Leparoux, A. Kawasaki, Dual-nanoparticle-reinforced aluminum matrix composite materials, Nanotechnology 23 (2012).
[13] S. Dhandapani, T. Rajmohan, K. Palanikumar, M. Charan, Synthesis and characterization of dual particle (MWCT + B_4C) reinforced sintered hybrid aluminum matrix composites, Part. Sci. Technol. 34 (2016) 255–262.
[14] E. Ghasali, P. Sangpour, A. Jam, H. Rajaei, K. Shirvanimoghaddam, T. Ebadzadeh, Microwave and spark plasma sintering of carbon nanotube and graphene reinforced aluminum matrix composite, Archives of Civil and Mechanical Engineering 18 (2018) 1042–1054.
[15] M. Rashad, F. Pan, A. Tang, M. Asif, M. Aamir, Synergistic effect of graphene nanoplatelets (GNPs) and multi-walled carbon nanotube (MW-CNTs) on mechanical properties of pure magnesium, J. Alloys Compd. 603 (2014) 111–118.
[16] S. Polat, Y. Sun, E. Cevik, H. Colijn, Microstructure and synergistic reinforcing activity of GNPs-B_4C dual-micro and nano supplements in Al-Si matrix composites, J. Alloys Compd. 806 (2019) 1230–1241.
[17] J.H. Martin, B.D. Yahata, E.C. Clough, J.A. Mayer, J.M. Hundley, T.A. Schaedler, Additive manufacturing of metal matrix composites via nanofunctionalization, MRS Communications 8 (2018) 297–302.
[18] A. Maho, S. Linden, C. Arnould, S. Detriche, J. Delhalle, Z. Mekhalif, Tantalum oxide/carbon nanotubes composite coatings on titanium, and their functionalization with organophosphonic molecular films: a high quality scaffold for hydroxyapatite growth, J. Colloid Interface Sci. 371 (2012) 150–158.
[19] A. Nieto, A. Bisht, D. Lahiri, C. Zhang, A. Agarwal, Graphene reinforced metal and ceramic matrix composites: a review, Int. Mater. Rev. 62 (2017) 241–302.
[20] ASM International, Standard Practice for Operating Salt Spray (Fog) Apparatus, West Conshohocken, PA, USA, (2011).
[21] Y. Li, X. Wang, S. Yin, S. Xu, Influence of particle initial temperature on high velocity impact process in cold spraying, Procedia Environ. Sci. 12 (2012) 298–304.
[22] S. Damari, L. Cullari, D. Laredo, R. Nadiv, E. Ruse, R. Sripada, O. Regev, Graphene and boron nitride nanoplatelets for improving vapor barrier properties in epoxy nanocomposites, Progress in Organic Coatings 136 (2019).
[23] X. Meng, J. Zhang, J. Zhao, Y. Liang, Y. Zhang, Influence of gas temperature and properties of cold spray 304SS coating, Journal of Materials Science & Technology 27 (2011) 809–815.
[24] Z. Zhang, F. Liu, E.-H. Han, L. Xu, Mechanical and corrosion properties in 3.5% NaCl solution of cold sprayed Al-based coatings, Surf. Coat. Technol. 385 (2020) 125372.
[25] J. Mitchell, N. Crow, A. Nieto, Effect of surface roughness on pitting corrosion of AZ31 Mg alloy, Metals 10 (2020) 651.
[26] A. Nieto, J.M. Zhao, Y.-H. Han, K.H. Hwang, J.M. Schoenung, Microscale tribological behavior and in vitro biocompatibility of graphene nanoplatelet reinforced alumina, J. Mech. Behav. Biomed. Mater. 61 (2016) 122–134.
[27] C. Hsieh, J. Chen, R. Kuo, T. Lin, C. Wu, Influence of surface roughness on water- and oil-repellant surfaces coated with nanoparticles, Appl. Surf. Sci. 240 (2005) 318–326.
[28] C. Xie, H. Li, X. Zhou, C. Sun, Corrosion behavior of cold sprayed pure zinc coating on magnesium, Surf. Coat. Technol. 374 (2019) 797–806.
[29] K. Xhanari, M. Finsgar, Organic corrosion inhibitors for aluminum and its alloys in chloride and alkaline solutions: a review, Arab. J. Chem. 12 (2019) 4646–4663.